Semiconductor laser design with an asymmetric large optical cavity waveguide and a bulk active layer near *p*-cladding for efficient high-power red light emission

To cite this article: Eugene A Avrutin and Boris S Ryvkin 2022 *Semicond. Sci. Technol.* **37** 125002

OPEN ACCESS
IOP Publishing
Semiconductor Science and Technology
Semicond. Sci. Technol. **37** (2022) 125002 (6pp)
https://doi.org/10.1088/1361-6641/ac985a

Semiconductor laser design with an asymmetric large optical cavity waveguide and a bulk active layer near *p*-cladding for efficient high-power red light emission

Eugene A Avrutin[1,*] **and Boris S Ryvkin**[2]

[1] School of Physics, Engineering, and Technology, University of York, York, United Kingdom
[2] A F Ioffe Physico-Technical Institute, St. Petersburg, Russia

E-mail: eugene.avrutin@york.ac.uk

Received 9 June 2022, revised 6 September 2022
Accepted for publication 7 October 2022
Published 20 October 2022

Abstract

A semiconductor laser design for efficient, high power, high brightness red light emission is proposed, using a large optical cavity asymmetric waveguide and a bulk active layer (AL) positioned very close to the *p*-cladding. The low threshold carrier density associated with the broad AL, as well as the proximity of the AL to the *p*-cladding, ensure that the electron leakage current, the major detrimental factor in red lasers, stays modest in a broad range of excitation levels. This in turn promises high-power, efficient operation.

Keywords: semiconductor laser, efficiency, visible

(Some figures may appear in colour only in the online journal)

1. Introduction

In the previous papers [1, 2], we proposed and analysed a high-power semiconductor laser design using an asymmetric large optical cavity (LOC) waveguide (with different refractive index steps at the interfaces between the optical confinement layer (OCL) and the *n*- and *p*-claddings, and a relatively thick (typically bulk) active layer (AL) positioned very near the *p*-cladding. Such a waveguide design combines a number of advantages. The broad asymmetric waveguide makes for reliable generation of a single transverse mode regardless of the lateral laser structure [1, 2], and also for a relatively narrow far field [2], hence high brightness. The asymmetric position of the AL (if necessary, helped by strong *n*-doping of the *n*-side of the waveguide [3]) helps minimise the accumulation of nonequilibrium carriers in the waveguide at high injection levels, which allows the internal losses in the laser to be kept down up to high currents, in turn helping the laser to maintain high output efficiency up to high injection levels. This was shown to be particularly important for lasers (with both bulk or quantum well (QW) ALs) operating at the long wavelengths ($\sim$1.5 μm) using InGaAsP quaternary materials, due to the large free hole absorption cross section in those materials [1, 4] but was also shown to be relevant for GaAs/AlGaAs based lasers operating at a wavelength around 0.85 μm [2]. Finally, the bulk AL, besides providing some extra flexibility in the waveguide design due to the waveguiding properties of the AL itself, also makes for a relatively low threshold carrier density. This makes it possible to use short-cavity laser design which is

* Author to whom any correspondence should be addressed.

useful for efficient high pulsed power, quasi-continuous wave operation (though not for true continuous wave (CW) operation, since short cavities are prone to substantial self-heating).

Recent experimental results confirm the advantages of this structure in minimising the internal loss effect and achieving high pulsed powers at the long wavelength (∼1.5 μm) [5, 6].

Here, we note that the same design strategy may also offer some advantages for high power lasers operating at evens shorter, visible (for example, red), wavelengths, though the rationale for these advantages is different from that studied previously for infrared lasers. Some of the considerations we employed for those lasers (single broad transverse mode in an asymmetric LOC structure) are readily portable to the red laser case. There is however one extra effect that needs to be considered, namely the leakage current from the AL to the *p*-cladding and the associated reduction in the injection efficiency, which was neglected in our previous work but is more of a danger in red lasers than in infrared ones due to lower potential barriers involved. A number of design solutions have been investigated since the 1990s for overcoming this limitation, almost exclusively using QW lasers (typically 1–3 wells). Firstly, it has been shown that the correct design of the red laser waveguide was very important, which includes optimising the waveguide thickness to avoid mode penetration into the lossy GaAs substrate [7], and also designing the thickness of the *p*-cladding layer large enough [8]. In addition, the use of multiquantum barriers (MQBs) at the interface between the OCL and the *p*-cladding was used to effectively increase the OCL/*p*-cladding energy barrier for electrons both at room temperature and elevated temperatures (see e.g. [9] and references therein).

Below, we shall show that the strongly asymmetric waveguide laser design with a bulk AL located very close to the *p*-cladding may be a viable alternative to those designs, while also offering a number of additional advantages.

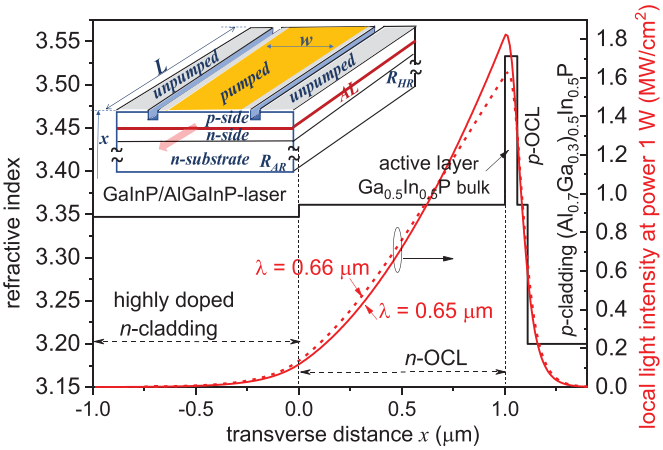

Figure 1. Schematic of the refractive index profile of the laser structure and the waveguide mode intensity distribution for the wavelength of 650 nm (solid), 660 nm (dashed). The inset shows a typical 3D structure possible, with the *n*-side comprising the *n*-cladding and the *n*-OCL and the *p*-side, the *p*-cladding and the *p*-OCL. Active stripe width $w = 100$ μm.

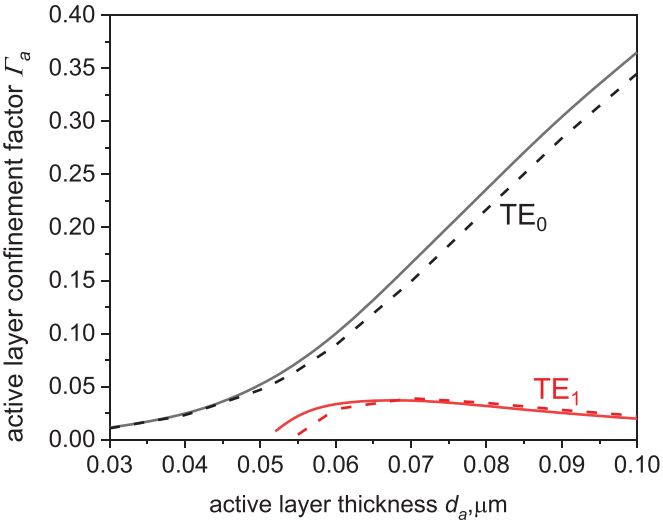

Figure 2. Confinement factors of the optical modes as function of the active layer thickness for the structure of figure 1: solid line: $\lambda = 650$ nm; dashed line—$\lambda = 660$ nm.

2. Laser structure

The refractive index profile of the structure considered is shown schematically in figure 1. It represents a visible-emitting $Ga_{0.5}In_{0.5}P/(Al_xGa_{1-x})_{0.5}In_{0.5}P$ (lattice matched to GaAs) laser with a bulk AL, with the same composition as in, for example, [10], but with a fully disordered (random) structure so designed to emit at $\lambda \approx 650$–660 nm (figure 1) at room temperature [11], depending on the threshold carrier density value. The relation between the material composition and the refractive index is determined from [12]. As in our previous work, and unlike the previously published work on red lasers with bulk ALs such as, e.g. [10], the waveguide used is a LOC strongly asymmetric one, with the refractive index step at the interface between the OCL and the *n*-cladding substantially smaller than that at the OCL/*p*-cladding interface. The bulk (GaInP) AL is positioned at a very short distance (≈50 nm) from the *p*-cladding.

The profile of the fundamental (TE0) transverse mode intensity is also shown in figure 1. For the structure shown (with the AL thickness $d_a = 600$ Å), the second (TE1) mode can, strictly speaking, be also supported but its confinement factor is so small (figure 2) that it is certain to pose no threat to single transverse mode laser operation. As in the previous work [1, 2], the dependence of the fundamental mode confinement factor Γ_a on the AL thickness d_a (figure 2) in a broad range of d_a values is superlinear, showing that the AL itself contributes to the waveguiding properties of the structure and to some extent shapes the mode. Note that penetration of the light intensity into the highly doped *p*-cladding layer is very small in our asymmetric waveguide structure, which is known to be necessary in order to reduce absorption in the *p*-cladding layer [7] and in the *p*-GaAs contact layer [8] in red-emitting lasers.

3. Analysis of laser efficiency

As is well known, highly efficient operation of a semiconductor laser requires, firstly, low parasitic losses (both built-in and injection-dependent) and, secondly, high injection efficiency (which in turn requires low electron current leakage into the *p*-cladding). As discussed in the Introduction, it has been already shown that the first of these effects is effectively suppressed (at any wavelength) in the double-asymmetric structure of the type shown here, with both bulk and QW AL [1–6, 13–16]. Therefore we shall concentrate on the second of the two considerations, the current leakage, which is known to be a significant threat in visible-range emitting lasers (see e.g. [8, 17, 18]).

The magnitude of the current leakage is determined by the quasi Fermi level separation in the AL, and hence sharply increases with the AL carrier density. Hence we start with calculating the threshold value of the carrier density in the AL as function of the AL thickness for the structure of figure 1. Since the AL is a bulk material, we use a simple linear dependence of the peak gain on the carrier density: $g(N) = \sigma_g(N - N_{tr})$, where the gain cross-section σ_g and the transparency carrier density, as functions of temperature T, were evaluated from microscopic calculations following [19, 20] (using a sech lineshape function). The results were approximated well by a linear dependence with $\sigma_g \approx 2.52 \times 10^{-16}$ cm^2, $N_{tr} \approx 2.0 \times 10^{18}$ cm^{-3} at $T = 300$ K and $\sigma_g \approx 2.20 \times 10^{-16}$ cm^2, $N_{tr} \approx 2.5 \times 10^{18}$ cm^{-3} at $T = 350$ K. Then the threshold carrier density, as usual, is

$$N_{th} = N_{tr} + \frac{\alpha}{\Gamma_a \sigma_g} \tag{1}$$

where Γ_a is the AL confinement factor and, as usual, the total cavity loss α includes both the internal and outcoupling loss: $\alpha = \alpha_{in} + \alpha_{out}$. Figure 3 shows the calculated threshold carrier density values for the two temperatures as functions of d_a. It is seen that for d_a values in excess of $d_a \approx 600$ Å, the threshold carrier density depends only weakly on d_a and is only slightly above the transparency value for the corresponding temperatures.

The threshold carrier density and the temperature determine the minority carrier (electron) density at the edge of the *p*-cladding, which directly scales the leakage current:

$$N_e^{(p)} = N_c^{(p)} \exp\left(-\frac{\delta E_{Fe}^{(p)}}{k_B T}\right). \tag{2}$$

Here $N_c^{(p)}$ is the effective density of states of electrons in the *p*-cladding material,

$\delta E_{Fe}^{(p)} = E_c^{(p)} - E_{Fe} > 0$ is the difference between the energy $E_c^{(p)}$ of the lowest subband of the conduction band of the *p*-cladding material and the absolute position of the electron quasi Fermi level [8, 17, 18]. The numerator of the ratio in the exponential is positive at all realistic parameter values and is determined from the conditions of continuity of both electron and hole quasi Fermi levels across the structure [8, 17, 18]

$$\delta E_{Fe}^{(p)} = E_g^{(p)} - \Delta E_F^{(a)} - \delta E_{Fh}^{(p)} \tag{3}$$

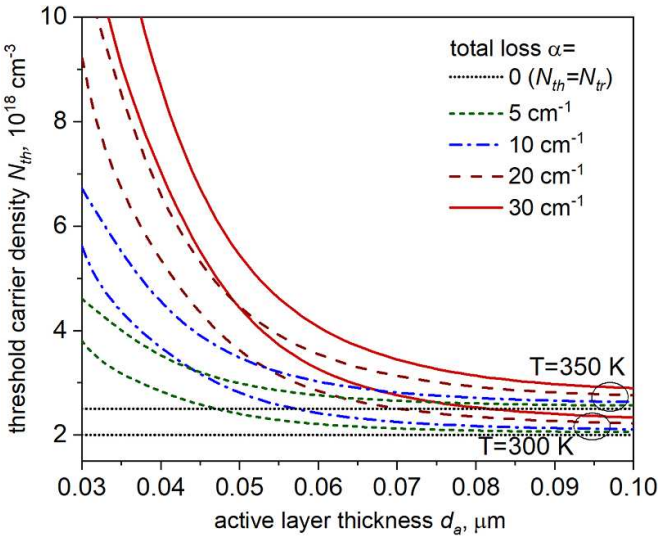

Figure 3. Threshold carrier densities in the structure of figure 1 for different values of the total cavity loss and temperature.

where $\Delta E_F^{(a)}$ is the electron and hole quasi Fermi level separation in the AL (calculated taking into account the AL bandgap shrinkage with carrier density and temperature), $E_g^{(p)}$ is the bandgap of the *p*-cladding (temperature dependent, with the room-temperature value taken from [8]), and $\delta E_{Fh}^{(p)} = E_{Fh}^{(p)} - E_v^{(p)} \approx k_B T \ln \frac{N_v^{(p)}}{N_A^{(p)}} > 0$ is the difference between the absolute position of the hole quasi Fermi level and the top of the valence band of the *p*-cladding material. It is determined by the density of the (ionised) acceptors (and hence the hole density) in the *p*-cladding $N_A^{(p)}$ and the effective density of states of holes in the *p*-cladding material $N_v^{(p)}$. The expression (3) assumes that spatially inhomogeneous accumulation of nonequilibrium carriers in the *p*-side of the OCL (*p*-OCL) is negligible, unlike the case of leakage current in structures with a large *p*-OCL thickness considered in [21]. This is ensured in our design by the very thin *p*-OCL (just 50 nm thick).

Figure 4 shows the calculated values of $\Delta E_F^{(a)}$ and the resulting values of $N_e^{(p)}$ as functions of the AL carrier density. It is clear that, even at an elevated temperature value, the minority (electron) density at the edge of the *p*-cladding remains very low if the AL carrier density is less than about 6×10^{18} cm^{-3}.

Moving on to evaluating the leakage effect as such, we note that, strictly speaking, the total leakage current density is the sum of diffusion and drift components [8, 17, 18]; however, in the case of AlGaInP lasers the leakage is known to be dominated by the drift leakage current, which is the electron current in the *p*-cladding [18]:

$$j_L = j_e^{(p)} = e\mu_e^{(p)} N_e^{(p)} F, \tag{4}$$

where e is the electron charge, $\mu_e^{(p)}$ is the minority electron mobility in the material of the *p*-cladding, F is the electric field in the *p*-cladding, and $N_e^{(p)}$ is given by equations (2) and (3).

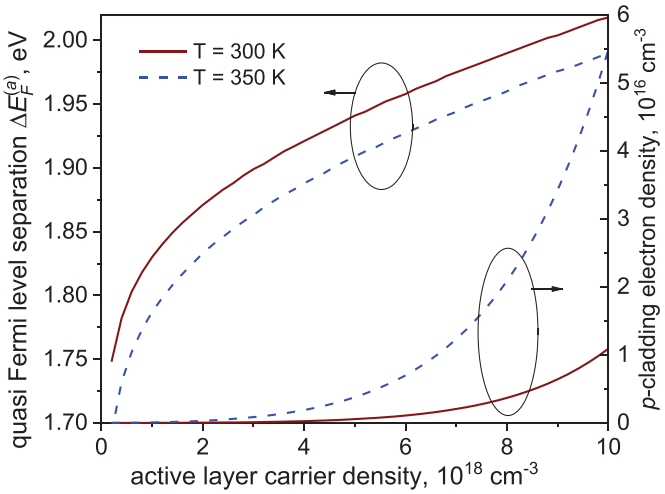

Figure 4. The electron and hole quasi Fermi level separation and the corresponding density of electrons thermally excited in the *p*-cladding for the designs of figures 1, 2 and different temperature values as function of active layer carrier density.

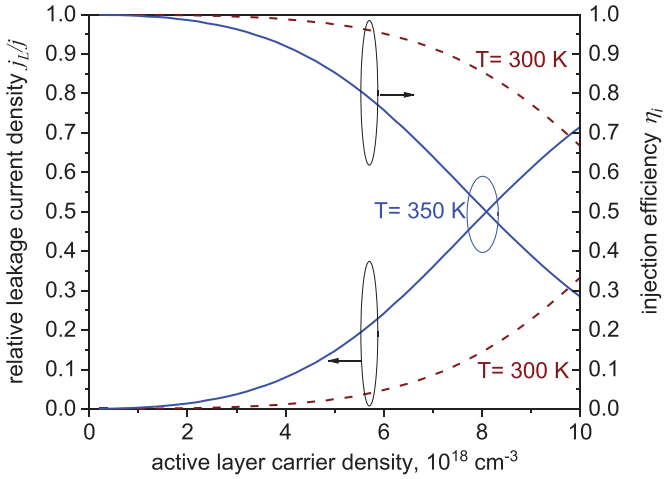

Figure 5. The leakage current as a fraction of the total current for the structure of figure 1 and two different temperature values as function of active layer carrier density.

This gives the electron to hole drift current density ratio in the *p*-cladding as

$$\Delta = \frac{j_e^{(p)}}{j_h^{(p)}} = \frac{e\mu_e^{(p)}N_e^{(p)}}{\sigma_h^{(p)}} = \frac{\mu_e^{(p)}}{\mu_h^{(p)}}\frac{N_e^{(p)}}{N_A^{(p)}}. \tag{5}$$

Here, $\sigma_h^{(p)} \approx e\mu_h^{(p)}N_A^{(p)}$ is the conductivity due to majority holes, $\mu_h^{(p)}$ being the hole mobility and $N_A^{(p)}$, again, the density of (ionised) acceptors that determines the hole density in the *p*-cladding.

In the literature, the ratio Δ is sometimes interpreted as the ratio of the leakage current density $j_L = j_e^{(p)}$ to the total current density j [8, 18], which is correct provided that $\Delta \ll 1$ (which is usually the case in situations of practical interest). More generally, since $j = j_e^{(p)} + j_h^{(p)}$,

$$\frac{j_L}{j} = \frac{\Delta}{1+\Delta}. \tag{6}$$

This allows the injection efficiency of the laser to be evaluated (neglecting carrier recombination in the OCL) in the form

$$\eta_i \approx 1 - \frac{j_L}{j} = \frac{1}{1+\Delta}. \tag{7}$$

Figure 5 shows the calculated values of the leakage current as a fraction of the total current (in other words, the ratio $j_e^{(p)}/j$) and the corresponding injection efficiency η_i for the structure of figure 1 and two different temperature values, as function of the AL carrier density. The values of $\mu_e^{(p)} = 160\ \text{cm}^2\,(\text{Vs})^{-1}$, $\mu_h^{(p)} = 7\ \text{cm}^2\,(\text{Vs})^{-1}$ are taken from [8] and it is assumed that the dominant scattering mechanism is the same for electrons and holes so the temperature dependence of the ratio $\mu_h^{(p)}/\mu_e^{(p)}$ within the relatively modest temperature variation range considered here (300–350 K) can be neglected.

As can be expected, temperature increase leads to a substantial increase in the leakage current and corresponding efficiency degradation.

Figure 6 shows the same two quantities as figure 5 but as functions of the AL thickness d_a with the threshold carrier density calculated from d_a using equation (1). At room temperature (figure 6(a)), noticeable degradation of efficiency by leakage is only seen for relatively high output losses (short cavity or low output reflectance); at elevated temperatures (figure 6(b)), the leakage becomes a concern even for modest output losses, particularly for thin active regions; however, for d_a in excess of about 600 Å (the value used in figure 1) the effect is rather small.

As regards the current dependence of efficiency, one notes that above threshold, the injection efficiency value given by equation (7) does not depend *explicitly* on current, only on the temperature. The internal losses α_{in}, and hence the output efficiency $\eta_{out} = \alpha_{out}/(\alpha_{in}+\alpha_{out}) = \alpha_{out}/\alpha$, of the laser design considered are also virtually independent on current, since the free carrier absorption by carriers accumulated in the OCL is negligible as discussed in the Introduction. Hence the calculated light-current curve of the laser in the quasi-CW regime (when self-heating can be neglected) is, in the first approximation, just the textbook straight line with a constant gradient given by the slope efficiency $\eta = \eta_{in}\eta_{out}$: $P_{out} \approx (\hbar\omega/e)\eta_i\eta_{out}(i - i_{th})$. More accurately, some increase in leakage, and hence some saturation of the output curve, can be expected due to non-pinning of the carrier density at the threshold value because of gain compression and, for a sufficiently low output facet reflectance values, also because of longitudinal spatial hole burning. However, these effects will be significant only at rather high currents. Under true CW operation, as with almost all semiconductor lasers, the output curve saturation can be expected to be mainly due to self-heating, since η_i decreases substantially with temperature (figure 5).

All calculations so far have been performed for a (fully random) $Ga_{0.5}In_{0.5}P$ AL. To get a better idea of possible applications, it is interesting to evaluate the possible

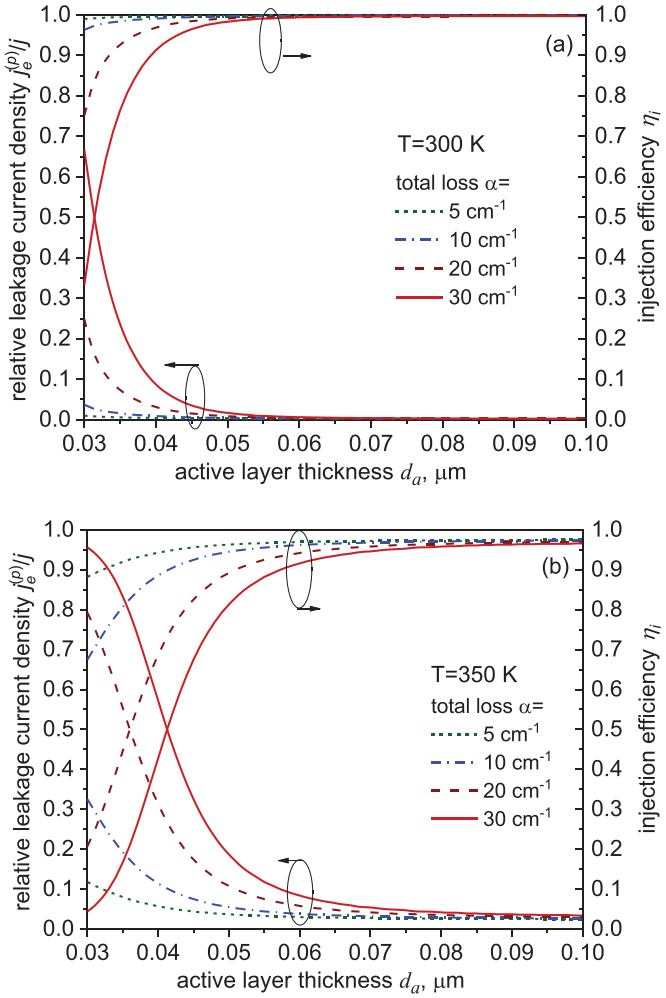

Figure 6. The ratio of the leakage to total current and the injection efficiency as functions of the active layer thickness for different values of the total cavity loss and the temperature 300 K (a) and 350 K (b).

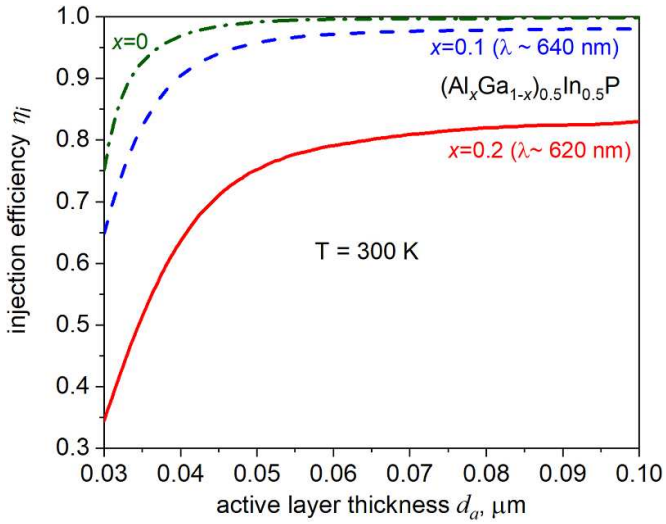

Figure 7. The injection efficiency as function of the active layer thickness at room temperature (300 K) for different material compositions. The total cavity loss is fixed at 20 cm^{-1}.

wavelength range that could be covered by lasers of this design by varying the AL composition. In principle, this can be achieved in two different ways. Firstly, it is possible to vary the fractions of Ga and In in the composition of the $Ga_{0.5+\delta}In_{0.5-\delta}P$ AL, which results in tensile or compressive strain in the material depending on the sign of δ [11]. This is a very useful instrument in designing a QW AL, but for our bulk, relatively thick, AL design this can potentially result in defects. Therefore, we have considered an alternative route, by introducing some aluminium in the material, described by the formula $(Al_xGa_{1-x})_{0.5}In_{0.5}P$. This way, the structure is kept lattice-matched throughout, avoiding the risk of defects. We have repeated the calculations described above for lasers with different AL compositions, ensuring different wavelength operation. In order to ensure that no significant carrier leakage occurs into the OCL, the composition of the OCL and the *n*-cladding was varied alongside that of the AL, to maintain the constant barrier height for electrons. The material parameters for different Al compositions were taken from [11, 12, 21].

The calculated efficiency values are shown in figure 7. For all compositions, the efficiency increases with increased active value thickness (and hence decreased threshold carrier density N_{th}) and saturates for large values of d_a when N_{th} approaches the transparency value N_{tr}—the absolute limit to which it can be reduced, determining a hard limit of the efficiency. Obviously, the efficiency decreases with the increased aluminium content and thus decreased operating wavelength, due to the lowered energy barrier between the AL and the *p*-cladding. It can be seen from the figure that, while for small values of the Al content parameter *x*, this efficiency decrease is quite gentle, it becomes relatively steep for *x* in excess of 0.2 ($x = 0.3$, not shown in the figure, results already in unpractically low values of η_i). Still, the current design should allow the wavelength range of about 620–660 nm to be covered. While we have not performed calculations for strained materials, using strain weak enough to not introduce defects may be expected to allow some additional broadening of this range.

We believe that the current structure is promising because it brings together several features successfully used previously, but in different designs. The first of these is the bulk AL, with a thickness of >∼400 Å, as in [10]. Note that the analysis in [10] concentrated exclusively on the threshold current; here, it has been shown that the injection efficiency can also be optimised by the appropriate design of a bulk AL—indeed, as discussed above, the bulk AL allows for a high confinement factor, leading to a relatively low threshold carrier density, which in turn results in a relatively low value of the quasi Fermi level separation and hence leakage current, leading to a high injection efficiency. This advantage, on its own, is not unique to the proposed design: injection efficiencies approaching one can also be achieved by QW lasers (see e.g. [7]) if a sufficiently high confinement factor and hence a relatively low threshold carrier density/quasi Fermi level separation is achieved. With the simple QW (1–3 wells) design, this would necessitate a narrow symmetric waveguide as in [7], figure 1 top). Such a narrow symmetric waveguide, however, necessarily results in a substantial overlap with the highly doped *p*-cladding (and in

the case of a thin *p*-cladding, also with the GaAs contact layer), leading to substantial optical losses [7, 8]. Besides, a narrow waveguide tends to allow only limited beam quality. The current design, on the other hand, utilises a *broadened* waveguide but with the additional benefits given by the strong waveguide asymmetry and the relatively thick AL. Those include, firstly, the low optical loss (despite the thin *p*-cladding, which is very beneficial in red emitting lasers [8]), secondly, strongly suppressed inhomogeneous carrier accumulation in the OCL (which would have been detrimental to injection efficiency [22, 23]) as already discussed in the Introduction, and, thirdly, a single, broad mode leading to low beam divergence/high brightness.

As regards the comparison of the current design with those QW (or bulk) lasers that employ MQB structures, both have been predicted to all but eliminate current leakage at room temperature and strongly suppress it at elevated temperatures, and both are, in principle, compatible with low optical losses. The potential advantage of the current design is that it is simple, robust, and avoids the use of multiple heterointerfaces which could lead to additional surface recombination (hence reduced injection efficiency) and electrical resistance (hence reduced wall-plug efficiency). In principle, the current structure can also be combined with a MQB.

Finally, it is worth noting that, although the primary purpose of this paper is analysing the specific design for visible-emitting lasers, the generalised analysis of leakage current and its effect on efficiency (equations (6) and (7)) is relatively generic and holds whenever the leakage current in a semiconductor laser is mainly drift in nature.

Data availability statement

The data that support the findings of this study are available upon reasonable request from the authors.

ORCID iD

Eugene A Avrutin https://orcid.org/0000-0001-5488-3222

References

[1] Ryvkin B S, Avrutin E A and Kostamovaara J T 2020 Asymmetric-waveguide, short cavity designs with a bulk active layer for high pulsed power eye-safe spectral range laser diodes *Semicond. Sci. Technol.* **35** 085008

[2] Avrutin E A, Ryvkin B S and Kostamovaara J T 2021 AlGaAs/GaAs asymmetric-waveguide, short cavity laser diode design with a bulk active layer near the *p*-cladding for high pulsed power emission *IET Optoelectron.* **15** 194–9

[3] Ryvkin B S, Avrutin E A and Kostamovaara J T 2017 Strong doping of the *n*-optical confinement layer for increasing output power of high-power pulsed laser diodes in the eye safe wavelength range *Semicond. Sci. Technol.* **32** 125008

[4] Ryvkin B S and Avrutin E A 2005 Asymmetric, nonbroadened large optical cavity waveguide structures for high-power long-wavelength semiconductor lasers *J. Appl. Phys.* **97** 123103

[5] Hallman L W, Ryvkin B S, Avrutin E A, Aho A T, Viheriala J, Guina M and Kostamovaara J T 2019 High power 1.5 μm pulsed laser diode with asymmetric waveguide and active layer near p-cladding *IEEE Photonics Technol. Lett.* **31** 1635–8

[6] Hallman L W, Ryvkin B S, Avrutin E A and Kostamovaara J T 2021 >25 W pulses from 1.5 μm double-asymmetric waveguide, 100 μm stripe laser diode with bulk active layer *Electron. Lett.* **57** 891–3

[7] Lichtenstein N, Winterhoff R, Scholz F, Heinz Schweizer S W, Reichl H, Reichl H and Reichl H 2000 The impact of LOC structures on 670-nm (Al)GaInP high-power lasers *IEEE J. Sel. Top. Quantum Electron.* **6** 564–70

[8] Smowton P M, Thomson J D, Yin M, Dewar S V, Blood P, Bryce A C, Marsh J H, Hamilton C J and Button C C 2002 The effect of cladding layer thickness on large optical cavity 650-nm lasers *IEEE J. Quantum Electron.* **38** 295–290

[9] Sobiesierski A, Sandall I C, Smowton P M, Blood P, Krysa A B, Brown M R, Teng K S and Wilks S P 2005 AlGaInP laser diodes incorporating a 3l/4 multiple quantum barrier *Appl. Phys. Lett.* **86** 021102

[10] Ishikawa M, Shiozawa H, Itaya K, Hatakoshi G and Uematsu Y 1991 Temperature dependence of the threshold for InGaAlP visible laser diodes *IEEE J. Quantum Electron.* **27** 23–29

[11] Bour D 1993 AlGaInP quantum well lasers *Quantum Well Lasers* ed P S Zory (San Diego, CA: Academic)

[12] Adachi S, Kato H, Moki A and Ohtsuka K 1994 Refractive index of $(Al_xGa_{1-x})_{0.5}In_{0.5}$ quaternary allows *J. Appl. Phys.* **75** 478–80

[13] Crump P *et al* 2013 Efficient high-power laser diodes *IEEE J. Sel. Top. Quantum Electron.* **19** 1501211

[14] Yamagata Y, Yamada Y, Muto M, Sato S, Nogawa R, Sakamoto A and Yamaguchi M 2015 915nm high power broad area laser diodes with ultra-small optical confinement based on asymmetric decoupled confinement heterostructure (ADCH) *Proc. SPIE* **9348** 93480F

[15] Hasler K H, Wenzel H, Crump P, Knigge S, Maasdorf A, Platz R, Staske R and Erbert G 2014 Comparative theoretical and experimental studies of two designs of high-power diode lasers *Semicond. Sci. Technol.* **29** 045010

[16] Kaul T, Erbert G, Maassdorf A, Martin D and Crump P 2018 Extreme triple asymmetric (ETAS) epitaxial designs for increased efficiency at high powers in 9xx-nm diode lasers *Proc. SPIE* **10514** 105140A

[17] Agrawal G P and Dutta N K 1986 *Long-wavelength Semiconductor Lasers* (New York: Van Nostrand Reinhold)

[18] Bour D P, Treat D W, Thornton R L, Geels R S and Welch D F 1993 Drift leakage current in AlGaInP quantum-well lasers *IEEE J. Quantum Electron.* **29** 1337–43

[19] Coldren L, Corzine S W and Masanovic M L 2012 *Diode Lasers and Photonic Integrated Circuits* (New York: Wiley)

[20] Rees P, Summers H D and Blood P 1991 Gain-current calculations for bulk GaInP lasers including many-body effects *Appl. Phys. Lett.* **59** 3521–2

[21] Rennie J, Okajima M, Watanabe M and Hatakoshi G-I 1993 High temperature (74 C) CW operation of 634 nm InGaAlP laser diodes utilizing a multiple quantum barrier *IEEE J. Quantum Electron.* **29** 1857–62

[22] Garbuzov D Z, Ovchinnikov A V, Pikhtin N A, Sokolova Z N, Tarasov I S and Khalfin V B 1991 Experimental and theoretical investigations of singularities of the threshold and power characteristics of InGaAsP/InP separate-confinement double-heterostructure lasers ($\lambda = 1.3$ μm) *Sov. Phys. Semicond.* **25** 560–4

[23] Ryvkin B S and Avrutin E A 2005 Effect of carrier loss through waveguide layer recombination on the internal quantum efficiency in large-optical-cavity laser diodes *J. Appl. Phys.* **97** 113106